J. Biochem. **144,** 305–312 (2008)
doi:10.1093/jb/mvn069

Crystal Structure of Pyruvate Kinase from *Geobacillus stearothermophilus*

Kenichiro Suzuki, Sohei Ito, Akiko Shimizu-Ibuka and Hiroshi Sakai*

Department of Food and Nutritional Sciences, Graduate School of Nutritional and Environmental Sciences, University of Shizuoka, Yada 52-1, Shizuoka 422-8526, Japan

Received March 14, 2008; accepted April 21, 2008; published online May 28, 2008

The pyruvate kinase (PK) from a moderate thermophile, *Geobacillus stearothermophilus*, is an allosteric enzyme activated by AMP and ribose 5-phosphate but not fructose 1, 6-bisphosphate (FBP), which is a common activator of PKs. It has an extra C-terminal sequence (ECTS), which contains a highly conserved phosphoenolpyruvate (PEP) binding motif, but its function and structure remain unclear. To elucidate the structural characteristics of the effector-binding site and the ECTS, the crystal structure of the C9S/C268S mutant of the enzyme was determined at 2.4 Å resolution. The crystal belonged to space group $P6_222$, with unit cell parameters a, $b = 145.97$ Å, $c = 118.03$ Å. The enzyme was a homotetramer and its overall domain structure was similar to the previously solved structures except that the ECTS formed a new domain (C′ domain). The structure of the C′ domain closely resembled that of the PEP binding domain of maize pyruvate phosphate dikinase. A sulphate ion was found in a pocket in the effector-binding C domain. This site corresponds to the 6-phosphate group-binding site in yeast PK bound FBP and seems to be the effector-binding site. Through comparison of the structure of the putative effector-binding site to that of the FBP binding site of the yeast enzyme, the structural basis of the effector specificity of the *G. stearothermophilus* PK is discussed.

Key words: allosteric, AMP, crystal structure, pyruvate kinase, ribose 5-phosphate.

Abbreviations: $A_{0.5}$, activator concentration required for half maximal activation; ECTS, extra C-terminal sequence; FBP, fructose 1, 6-bisphosphate; GstPK, *Geobacillus stearothermophilus* pyruvate kinase; GstPKNC, *Geobacillus stearothermophilus* pyruvate kinase C9S/C268S mutant; PEP, phosphoenolpyruvate; PK, pyruvate kinase; PPDK, maize pyruvate phosphate dikinase; R5P, ribose 5-phosphate; $S_{0.5}$, substrate concentration required for half maximal saturation.

Pyruvate kinase (PK; EC 2.7.1.40) catalyzes the final step of glycolysis, the phosphoryl group of phosphoenolpyruvate (PEP) being transferred to ADP to yield pyruvate and ATP (*1*, *2*). This reaction is essentially irreversible and is one of the major control points in glycolysis. The PKs from a number of prokaryotes and eukaryotes have been isolated and characterized. Most of them exist as tetramers of identical subunits (*1*, *3*, *4*). The crystal structures of the cat, rabbit muscle, human erythrocyte, yeast, *Escherichia coli* and *Leishmania mexicana* PKs have been reported, and their overall structures are similar (*5–9*). Each subunit of the tetramer consists of four domains: A, B, C and N-terminal domains. The N-terminal domain is only found in mammalian enzymes and all the prokaryotic enzymes lack this domain. The A domain, located between the B and C domains, has a (β/α)8 structure. The active site lies at the interface of the A and B domains in each of the four subunits. In the yeast and erythrocyte PKs, the binding site for an allosteric effector is completely located in the C domain (*6*, *7*).

Almost all PKs are activated by fructose 1, 6-bisphosphate (FBP). The PK from *Geobacillus stearothermophilus* (GstPK) is, however, allosterically activated by AMP and ribose 5-phosphate (R5P) but not by FBP. The enzyme is very stable at high temperature, in spite of the instability of other microbial PKs (*10*). The PKs from genus *Geobacillus* and some other bacteria have a long extra C-terminal sequence (ECTS) composed of about 110 amino acid residues (*11–15*). A part of this sequence is highly homologous to that of the PEP-binding motif. It is suggested that the ECTS weakly interacts with the A domain and C domain (*16*). The ECTS may play some role in the structural stability of the enzyme.

We have tried to crystallize GstPK to determine its crystal structure, and to determine the structural bases of the effector specificity and the ECTS structure. The wild-type and W416F/V435W mutant GstPK were crystallized, but they were unsuitable for structural analysis because of the low completeness value of their dataset (*17*). GstPK has two cysteine residues (C9 and C268). These two residues were mutated to serines, and the resultant mutated enzyme was designated as GstPKNC (*18*). GstPKNC gave a crystal suitable for structural analysis. In this report, we describe the structure of GstPKNC. This is the first report on the structure of a PK having the ECTS and that is allosterically activated by AMP and R5P.

*To whom correspondence should be addressed. Tel: +81-54-264-5576, Fax: +81-54-264-5099,
E-mail: gp1314@mail.f.u-shizuoka-ken.ac.jp

MATERIALS AND METHODS

Protein Expression and Purification—The wild-type GstPK and two mutants were expressed and purified as described previously (*16*). Plasmid pKHNC, which comprised pKH510 with the C9S/C268S mutation introduced, was employed for GstPKNC production (*18*). PK-deficient *E. coli* mutant PB25 (*pyrA*::*kan pyrF*::*cat*) was generously donated by Dr E. Ponce and used as the host cells in this experiment (*19*). *Escherichia coli* mutant PB25 harbouring plasmid pKHNC was cultivated at 37°C in Luria–Bertani broth containing 100 μg/ml of ampicillin with an inoculum of 1% of an overnight culture. Three hours later, isopropyl-l-thio-β-D-galactopyranoside was added to 0.5 mM and the cultivation was continued for 16–8 h. Cells were harvested by centrifugation, suspended in five volumes of 25 mM Tris–HCl, pH 7.5, containing 150 mM NaCl and then disrupted with a Sonifier ultrasonic disruptor (Branson, CT, USA). The enzymes were purified by means of Butyl–Toyopearl 650S (Tosoh, Japan) and Resource Q column (Amersham Biosciences, United Kingdom) chromatography. The purified GstPKs were dialyzed against 5 mM Tris–HCl buffer, pH 7.5, and then concentrated to 10–15 mg/ml using a Centricon YM-30 (Millipore). About 60 mg of purified GstPK was obtained from 1 l LB culture.

Enzymatic Assay—PK activity was measured by means of a coupling assay method using lactate dehydrogenase (LDH) (*10*). The assay mixture consisted of 50 mM imidazole-HCl (pH 7.2), 7 mM $MgCl_2$, 100 mM KCl, 0.25 mM nicotinamide adenine dinucleotide (NADH) and one unit of LDH per 0.2 ml assay mixture. To measure PEP saturation, the ADP concentration was fixed at 0.4 mM, which was far from saturation, but was chosen to minimize the effect of possible contamination by AMP of the ADP preparation. To measure the allosteric activation by R5P or AMP, the ADP and PEP concentrations were fixed at 0.5 and 0.4 mM, respectively. The velocities thus obtained were fitted to the Michaelis–Menten equation or Hill's equation by means of non-linear regression, and the kinetic parameters were calculated using a Kaleidagraph (Synergy Software, Reading, PA).

Crystallization—The protein was crystallized as described previously (*17*). Crystals suitable for data collection were obtained with a reservoir solution comprising 2.1 M ammonium sulphate and 0.1 M MES, pH 6.5, at 285 K at the protein concentration of 15 mg/ml. Crystals grew in one to two weeks.

X-ray Diffraction Experiments—Diffraction data for GstPKNC were collected at 2.4 Å resolution at beamline NW12, Photon Factory, Advanced Ring (PF-AR), Tsukuba, Japan. The crystals were soaked for a few minutes in mother liquor containing 20% (v/v) glycerol and then flash frozen in liquid nitrogen. Diffraction data were collected with a Quantum 210 CCD X-ray detector (Area Detector Systems Corporation, Poway, CA, USA). The dataset was processed and scaled using programs DENZO and SCALEPACK in the HKL 2000 package (*20*) (Table 1). The V_M values (*21*) and solvent contents of GstPKNC were calculated to be 2.91 $Å^3$/Da and 57.8%, respectively, assuming one tetrameric protein molecule per asymmetric unit.

Table 1. **Data-collection and refinement statistics for GstPKNC.**

X-ray wavelength (Å)	1.000
Space group	$P6_222$
Unit cell parameters	
a (Å)	145.97
b (Å)	145.97
c (Å)	118.03
	α, β = 90.0°, γ = 120.0°
Resolution (Å)	50 – 2.4 (2.49 – 2.40)
No. of observations	821,411
No. of unique reflections	28,179
Completeness (%)	97.7 (79.9)
R_{merge} (%)	5.5 (32.2)
Mean I/σ (I)	16.7 (6.1)
Refinement	
R-factor (%)	22.6
R_{free} (%)	29.4
R.m.s deviations	
Bond length (Å)	0.008
Bond angels (°)	1.44

Values in parentheses are for the last resolution shell.

Structure Determination—The GstPKNC structure was determined by molecular replacement with Molrep (ccp4i) using the structure of *E. coli* PKI as a search model (PDB ID: 1PKY) (*22*). The conditions for the data collection and refinement statistics are presented in Table 1. The structure was refined by simulated annealing and B-factor adjustments using program CNS (*23*), with iterative manual adjustment of the model using program O (*24*). The number of water molecules added to the model was 156. The final *R* factor for the model was 22.6%, with a R_{free} value of 29.4% at 2.4 Å resolution.

Accession Code—The coordinates and structure factors have been deposited in the Protein Data Bank under accession code 2E28.

Preparation of GstPK Mutants—Site-directed mutagenesis was performed for recombinant expression plasmid pKH510 (*10*). Mutations were introduced by means of the polymerase chain reaction Megaprimer method (*25*, *26*).

The oligonucleotide primers used for the H425A, V435R, V435K and V435E mutations were 5′-GAAAGAAGC<u>GCCG**GC**</u>TGTGAACACGACG-3′, 5′-GAAATGCTCGAT**CG** CGC C<u>GTCGA**C**</u>GCGGCGGTGCGC-3′, 5′-GAAATGCTCGAT**A AA**GCC<u>GTCGA**C**</u> G CGGCGGTGCGC-3′ and 5′-GAAATG CTCGATG**AA**GCC<u>GTCGA**C**</u>GCGGCGGTGC GC-3′, respectively. The underlined sequences indicate the introduced restriction sites and the mutated bases are expressed in boldface. The introduction of each mutation and the absence of an undesired mutation were confirmed by DNA sequencing. The mutant enzymes were purified and assayed as described earlier.

RESULTS

Overall Structure—The structure of GstPKNC was determined at 2.4 Å resolution as described under MATERIALS AND METHODS section. A single subunit and the tetrameric structure of GstPKNC are shown

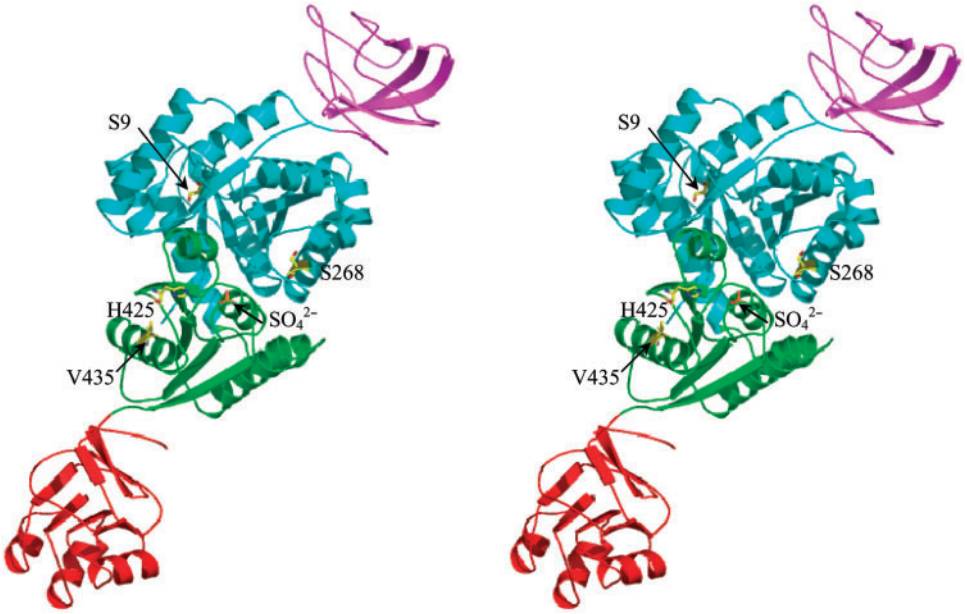

Fig. 1. **Ribbon diagram of the overall GstPKNC monomer.** His425, Val435 and the sulphate ion are shown as a ball and stick model. Domains A, B, C and C′ are shown in cyan, magenta, green and red, respectively. This figure and other figures were prepared with PyMOL (*32*).

schematically in Figs 1 and 3A, respectively. GstPKNC was a homotetramer and its overall conformation was similar to the previously solved structures. Each subunit of GstPK was composed of four separate domains (Fig. 1). The first domain, A, was supposed to be the catalytic domain and was formed by two separate stretches of amino acids (residues 1–70 and 170–360) that fold together into a common parallel $(\beta/\alpha)_8$ barrel motif with two additional α helices. The mutated residues, S9 and S268, were buried deeply in the A domain. The second domain, B, a capped domain (residues 71–169), comprised a small four-stranded β-barrel motif that formed a cap over the active site. The third domain, C, comprised an α/β open-sheet motif and contained an allosteric effector binding site (residues 361–470). Finally, the ETCS formed a new domain. This new domain was located at the C terminus of the protein (residues 477–587) and was named the C′ domain. The four domains were aligned almost linearly in the order of B, A, C and C′. The position of the C′ domain was slightly displaced from the axis formed by the centres of the B, A and C domains, which enabled face to face contact between neighbouring C domain (Fig. 3A).

C-terminal Sequence and C′ Domain Structure—It has been reported that the PKs from *G. stearothermophilus* (*11*), *B. subtilis* (*14*), *B. licheniformis*, *L. delbrueckii*, *B. psychrophilus* and cyanobacteria *Synechocystis* sp have an ECTS. In GstPK for example, this sequence consists of ~110 amino acid residues and includes a highly conserved PEP-binding motif (*11*).

This motif is found in *E. coli* and *Salmonella typhimurium* PEP-sugar phosphotransferase system enzyme I, maize pyruvate phosphate dikinase (PPDK) and *E. coli* PEP synthase (*11*, *27*, *28*). In these enzymes, the PEP-binding motif is highly conserved principally

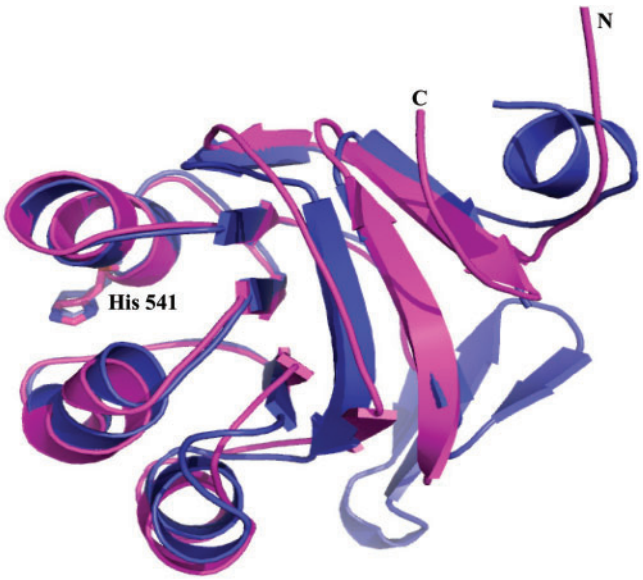

Fig. 2. **Cα superpositioning of the GstPKNC C′ domain (red) and the PPDK phosphohistidine domain (blue).** The His541 residue of GstPKNC is shown as a ball-and-stick model and His455 of PPDK is shown as a wire frame.

around the histidyl residue, which is phosphorylated during the enzymatic reaction. The C′ domain in GstPK has been suggested to be derived from a PEP synthase late in the evolutionary process (*27*).

The C′ domain spans residues 477–587, and its structure closely resembles that of the PPDK phosphohistidine domain (Cα root mean square deviation, 2.79 Å. Fig. 2). It consists of 3- and 5-stranded orthogonal β-sheets (Fig. 2). These two β-sheets are antiparallel.

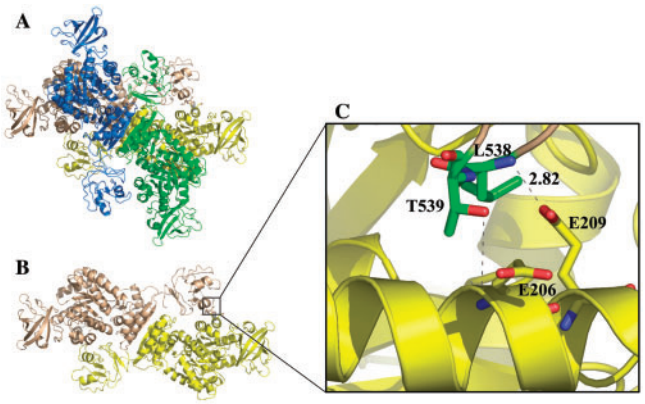

Fig. 3. **Overall structure of tetrameric GstPK, and interaction of the GstPKNC C′ domain and the A domain at the subunit interface.** (A) Ribbon diagram of the GstPKNC tetramer structure. The monomer is coloured blue, green, yellow and wheat. (B) The structure with two monomers removed (green and blue). (C) Close-up view of the C′–A domain interface. The area in the small square in B is magnified.

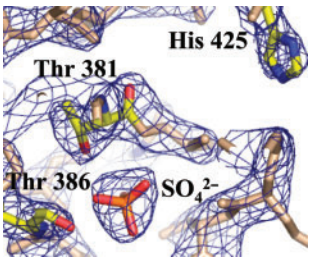

Fig. 4. **Electron density map of the region around the sulphate ion binding site of the C domain of GstPKNC.** The electron density map (2*Fo*–*Fc*) is shown in blue (1.5σ contour). Thr381, Thr386, His425 and the sulphate ion are shown as a ball-and-stick model.

The three-layer β/β/α architecture has been proposed to be as a folding class in SCOP (*29*). The fold of the phosphohistidine domain of PPDK (*30*) remotely resembles that of aconitase (*31*).

Interaction between the A Domain and C′ Domain at the Subunit Interface—Some weak interactions between the C′ domain and A domain, and the C′ domain and C domain have been postulated based on the results of kinetic analysis of the C-terminally truncated enzyme (*16*). Figure 3C shows the subunit interface between the C′ domain and A domain of neighbouring subunits. It seems that the amido nitrogen of Leu538 in the C′ domain and the carboxyl oxygen of Glu209 in the A domain form a hydrogen bond (distance, 2.82 Å) (Fig. 3C). No significant interaction was found between the C' domain and C domain.

R5P-Binding Site—Jurica *et al*. and Valentini *et al*. reported the structures of yeast PK and human erythrocyte PK complexed with a substrate analog and a catalytic metal ion in the presence and absence of bound FBP, respectively. In these PKs, the 6-phosphate group of bound FBP is tightly held by three hydroxyl groups provided by two Ser and one Thr. In GstPK, this position was occupied by a sulphate ion, and was coordinated similarly by three hydroxyl groups (Thr381, Ser383 and Thr386) (Fig. 4). The occupancy of a sulphate ion at the corresponding position has also been observed in *E. coli* PKI and *L. mexicana* PK. Thus, this sulphate ion binding site is thought to be a part of the effector-binding site. Many PKs are allosterically activated by FBP, but GstPK is activated by R5P and AMP. It is expected that the structure of the allosteric effector-binding site of GstPK differs from that of other PKs.

Site-directed Mutagenesis—In yeast PK, the allosteric effector-binding site is formed by a pocket in the C domain. The 1-phosphate group of FBP exhibits a strong 2.8 Å electrostatic interaction with a guanidino group of Arg459. In the GstPK structure this Arg459 corresponds to Val435. His425 is located in the loop between Cβ3 and

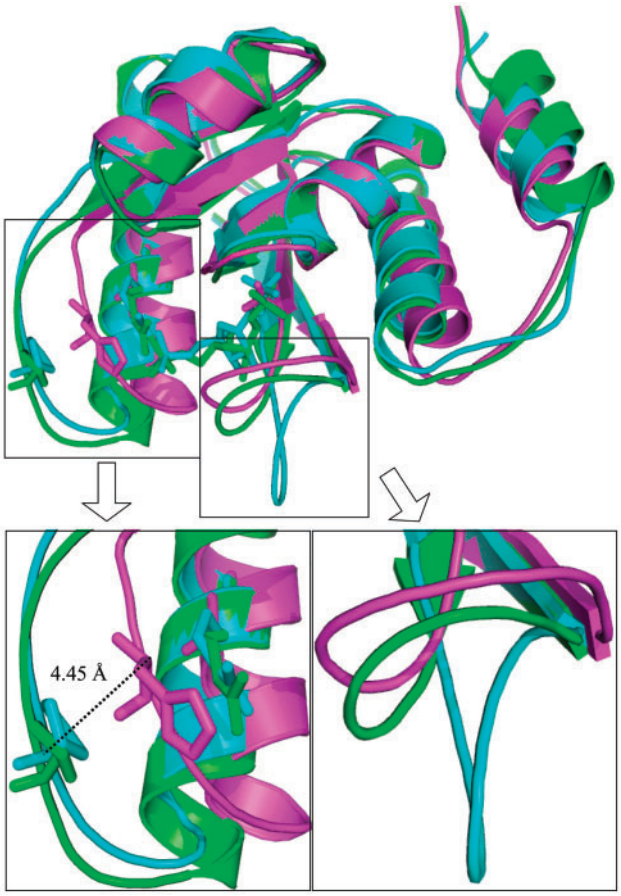

Fig. 5. **Cα superpositioning of the C domains of GstPKNC (magenta), yeast PK (cyan) and human erythrocyte PK (green), and a close-up view of the Cβ4–Cβ5 loop (right) and Cβ3–Cα5 loop (left).** The His425 and Val435 residues of GstPKNC, the Pro521 and Arg532 ones of human erythrocyte PK, the Pro449 and Arg459 ones of yeast PK, FBP bound to human erythrocyte PK and yeast PK and the sulphate ion bound to GstPKNC are shown as a ball-and-stick model. The distance between the Cα atom of His425 of GstPK and corresponding Cα atom of Pro449 of yeast PK is shown.

Cα5 of GstPK, and exists at the position considered to be the entrance of the effector-binding site (Fig. 5).

These four residues were subjected to mutagenesis (V435R, V435K, V435E and H425A). The mutated

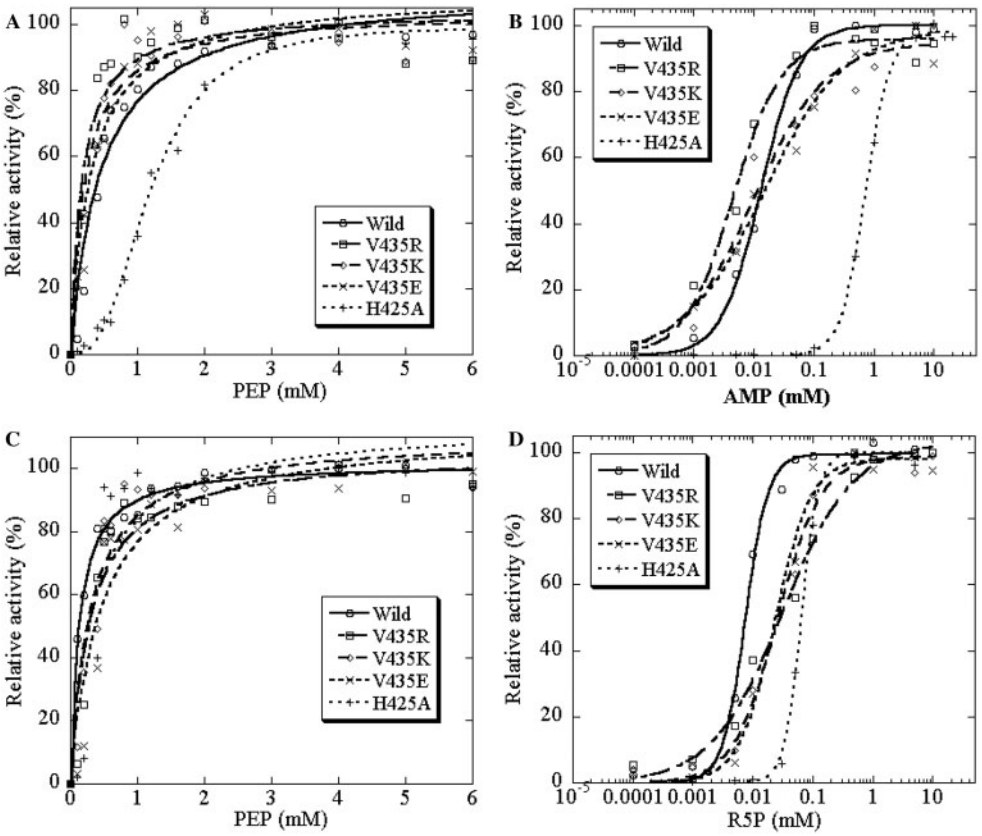

Fig. 6. **PEP saturation, and AMP and R5P activation profiles for wild-type GstPK and the four mutants.** (A) PEP saturation curves in the presence of 0.2 mM AMP. (B) AMP activation curves. The PEP concentration was fixed at 0.5 mM. (C) PEP saturation curves in the presence of 0.2 mM R5P. (D) R5P activation curves. The PEP concentration was fixed at 0.5 mM. Other assay conditions were given under MATERIALS AND METHODS section.

Table 2. **Kinetic parameters of the wild-type and H425A mutant.**

$S_{0.5}$ or $A_{0.5}$	Condition	Wild-type	H425A
$S_{0.5}$ (mM)	R5P (0.2 mM)	0.13 ± 0.02	0.41 ± 0.01
Vmax (U/mg)		204.9 ± 5.8	167.1 ± 2.5
$S_{0.5}$ (mM)	AMP (0.2 mM)	0.14 ± 0.01	1.21 ± 0.05
Vmax (U/mg)		217.3 ± 5.3	149.4 ± 3.8
$S_{0.5}$ (mM)	AMP (4.0 mM)	0.13 ± 0.01	0.36 ± 0.03
Vmax (U/mg)		197.2 ± 6.8	106.9 ± 4.1
$A_{0.5}$ (mM) for R5P	PEP (0.5 mM)	7.5×10^{-3}	6.5×10^{-2}
Vmax (U/mg)		202.4 ± 3.6	128.8 ± 2.4
$A_{0.5}$ (mM) for AMP	PEP (0.5 mM)	1.3×10^{-2}	0.74 ± 0.03
Vmax (U/mg)		182.1 ± 2.4	96.6 ± 1.3

enzymes were overexpressed in *E. coli* PB25 cells. The PEP saturation curves and activation profiles of AMP and R5P for V435 mutants are shown in Fig. 6. The $A_{0.5}$ values for R5P of the V435R, V435K and V435E mutants were increased about 4-fold, compared with that of the wild-type enzyme. The $A_{0.5}$ values for AMP and the $S_{0.5}$ values were essentially identical. This indicates that V435 does not play a major role in effector binding. The kinetic parameters for the H425A mutant were determined as described under EXPERIMENTAL PROCEDURES section and are shown in Table 2. The $S_{0.5}$ value of the H425A mutant in the presence of 0.2 mM AMP and R5P was increased 8.6- and 3.2-fold, respectively (Fig. 6 and Table 2). Additionally, the saturation curve in the presence of 0.2 mM AMP was still sigmoidal (Fig. 6A). Therefore, we measured the activation profiles of R5P and AMP. The $A_{0.5}$ values for H425A were increased 8.0- and 60-fold for R5P and AMP, respectively (Fig. 6B and D). The larger decrease in the affinity for AMP may indicate interaction between the imidazole group of His425 and the adenine ring of AMP.

DISCUSSION

The overall structures of a single subunit and the tetrameric form of GstPKNC were similar to the previously solved structures of PKs from other sources except for having a new domain. The ECTS, which contained a PEP-binding motif, formed a new domain, the C′ domain (Figs 1 and 2). The structure of this domain resembled that of the phosphohistidine domain of PPDK (Fig. 2). This suggest that the C′ domain plays some functional role in the PK activity or its regulation. A mutagenetic study, however, suggested that ECTS has no apparent functional role in the enzymatic activity or the enzyme's allosteric

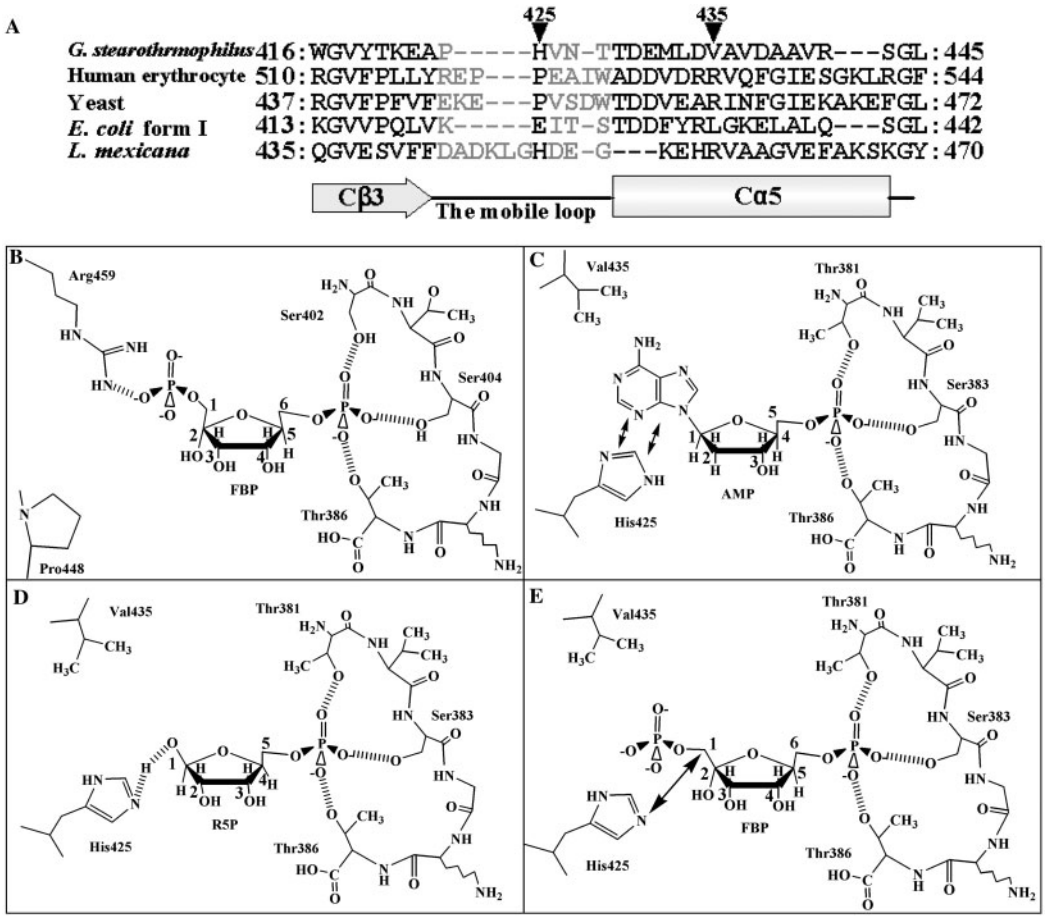

Fig. 7. **Schematic presentation of the effector recognition by yeast PK and GstPK**. (A) Structure-based alignment of the GstPK, human erythrocyte PK, yeast PK, *E. coli* form I and *L. mexicana* sequences. The secondary structure elements of these PKs are depicted below, as squares for α-helices and arrows for β-sheets. The Cβ3–Cα5 loop (the mobile loop) region is shown in gray. His425 of GstPK and the corresponding residues in other PKs, and Val435 of GstPK and the corresponding residues in other PKs are shown in arrows. (B) Schema of the FBP-binding interaction in yeast PK (*7*). (C) Plausible interactions when AMP is accommodated in the GstPK effector site. (D) When R5P is accommodated in this site. (E) In the case when FBP is accommodated.

characteristics but may play some role in thermal stability (*16*). A hydrogen bond found between the A domain and the C′ domain of the neighbouring subunit may slightly stabilize the structure and contribute to the thermostability of the enzyme (Fig. 3). The PEP-binding motif found in the ECTS and the structural similarity to the phosphohistidine domain of PPDK led us to imagine that it may once have played some role in the evolution of PK.

As shown in Fig. 4, a sulphate ion was found in the C domain and the site corresponded to the binding site for the 6-phosphate group of FBP. This position is thought to be the effector-binding site of GstPK.

The structure of the C domain of GstPK was compared with those of FBP-bound yeast PK and human erythrocyte PK. Two positions with significantly different conformations were found. One is the loop between Cβ4–Cβ5. The conformations of the loop of GstPK and human erythrocyte PK are essentially identical, but the loop of yeast PK is located about 5 Å away from the loops of GstPK and human erythrocyte PK. The difference in the position of the loop may not be due to the bound FBP, because the positions of the loop of the *E. coli*, *L. mexicana* and rabbit muscle PKs (*6*, *8*, *9*) in the absence of an effector were very similar to that of GstPK. The loop may be very flexible.

Another difference was found in the loop between Cβ3 and Cα5. This loop is one of the most variable parts of PK, and differs in both length and amino acid sequence. The corresponding loop in yeast PK comprises eight residues instead of the only five residues in GstPK (Fig. 7D). In yeast PK and human erythrocyte PK, it seems that FBP cannot interact with amino acid residues in the Cβ3–Cα5 loop since the loop is far from the bound FBP. On the other hand, in GstPK, this loop is short and close to a putative effector-binding site compared with in yeast PK and human erythrocyte PK. The distance between the Cα atom of His425 of GstPK and the corresponding Cα atom of Pro449 of yeast PK is 4.45 Å (Fig. 5). When His425 in this loop was replaced by Ala, the affinity for the allosteric activators was greatly decreased. The degree of the decrease was greater for AMP than for R5P. This may indicate that the adenine

ring of AMP interacts with the imidazole ring of His425. Other PKs activated by AMP and R5P, such as those of *B. licheniformis*, *B. psychrophilus*, *L. lactis* and *L. delbrueckii*, have His or Lys at this position. On the other hand, in yeast and human erythrocyte PKs, the loops are longer and far from the effector-binding site thus cannot participate in effector binding. Arg459 of yeast PK and Arg532 of human erythrocyte PK, however, extend their side chains from Cα5 and form a salt bridge with the 1-phosphate group of FBP. The amino acid residue in GstPK corresponding to these arginines is Val435. The kinetic properties of mutant PKs V435R, V435K and V435E were essentially identical to those of the wild-type enzyme. This indicates that Val435 does not participate in the effector recognition.

Kinetic analysis of the H425A mutant suggested that there are some interactions between His425 and allosteric effectors. The aromatic ring interaction between the adenine ring of AMP and the imidazole ring of His425 may be important for effector binding (Fig. 7C). Another possible interaction is the hydrogen bond formed between a nitrogen atom of the imidazole moiety and the atom bound at the 1-position of the sugar part of the effector (Fig. 7D). In the case of FBP, the atom is a non-polar methylene carbon and may not interact with the side chain of His425 (Fig. 7E). This may explain the effector specificity of GstPK.

In *E. coli* PK, which is activated by FBP but not by AMP or R5P, the effector recognition mechanism seems fairly different from that of the yeast enzyme. Arg459, which forms a salt bridge with the 1-phosphate of FBP, corresponds to Leu432 in the *E. coli* enzyme. The only positively charged amino acid residue near Leu432 is Arg431. Valentini *et al*. mutated this residue to glutamic acid and then kinetically analysed the mutant. There were no apparent differences in the allosteric activation (*2*). The Cβ3–Cα5 loop of the *E. coli* enzyme is short and this loop may be important for effector recognition, as in the case of GstPK. The residue corresponding to His425 of GstPK is Glu 422. This residue seems unfavourable for the binding of the negatively charged phosphate moiety of FBP. Lys 421 neighbouring Glu422 may play some role in FBP binding.

More details of the mechanism underlying allosteric regulation will be revealed by determining the crystal structure of the complex of GstPK and an allosteric effector.

REFERENCES

1. Kayne, F.J. (1973) Pyruvate kinase in *The Enzymes* (Boyer, P.D., ed.) Vol. 8, pp. 353–382
2. Valentini, G., Chiarelli, L., Fortin, R., Speranza, M.L., Galizzi, A., and Mattevi, A. (2000) The allosteric regulation of pyruvate kinase. *J. Biol. Chem.* **275**, 18145–18152
3. Schramm, A., Siebers, B., Tjaden, B., Brinkmann, H., and Hensel, R. (2000) Pyruvate kinase of the hyperthermophilic crenarchaeote *Thermoproteus tenax*: physiological role and phylogenetic aspects. *J. Bacteriol.* **182**, 2001–2009
4. Fothergill, L.A., Rigden, D.J., Michels, P.A.M., and Phillips, S.E.V. (2000) *Leishmania* pyruvate kinase: the crystal structure reveals the structural basis of its unique regulatory properties. *Biochem. Soc. Trans.* **28**, 186–190
5. Stuart, D.I., Levine, M., Muirhead, H., and Stammers, D.K. (1979) Crystal structure of cat muscle pyruvate kinase at a resolution of 2.6 Å. *J. Mol. Biol.* **134**, 109–142
6. Larsen, T.M., Laughlin, L.T., Holden, H.M., Rayment, I., and Reed, G.H. (1994) Structure of rabbit muscle pyruvate kinase complexed with Mn^{2+}, K^{+}, and pyruvate. *Biochemistry* **33**, 6301–6309
7. Jurica, M.S., Mesecar, A., Heath, P.J., Shi, W., Nowak, T., and Stoddard, B.L. (1998) The allosteric regulation of pyruvate kinase by fructose-1, 6-bisphosphate. *Structure* **6**, 195–210
8. Speranza, M.L., Valentini, G., Iadarola, P., Stoppini, M., Malcovati, M., and Ferri, G. (1989) Primary structure of three peptides at the catalytic and allosteric sites of the fructose-1, 6-bisphosphate-activated pyruvate kinase from *Escherichia coli*. *Biol. Chem. Hoppe Seiler.* **370**, 211–216
9. Rigden, D.J., Phillips, S.E.V., Michels, P.A.M., and Fothergill-Gilmore, L.A. (1999) The structure of pyruvate kinase from *Leishmania mexicana* reveals details of the allosteric transition and unusual effector specificity. *J. Mol. Biol.* **291**, 615–635
10. Sakai, H., Suzuki, K., and Imahori, K. (1986) Purification and properties of pyruvate kinase from *Bacillus stearothermophilus*. *J. Biochem.* **99**, 1157–1167
11. Sakai, H. and Ohta, T. (1993) Molecular cloning and nucleotide sequence of the gene for pyruvate kinase of *Bacillus stearothermophilus* and the production of the enzyme in *Escherichia coli*. *Eur. J. Biochem.* **211**, 851–859
12. Tanaka, K., Sakai, H., Ohta, T., and Matsuzawa, H. (1995) Molecular cloning of the genes for pyruvate kinases of the two bacilli, *Bacillus psychrophilus* and *Bacillus licheniformis*, and comparison of the properties of the enzymes produced in *Escherichia coli*. *Biosci. Biotechnol. Biochem.* **59**, 1536–1542
13. Kaneko, T., Sato, S., Kotani, H., Tanaka, A., Asamizu, E., Nakamura, Y., Miyajima, N., Hirosawa, M., Sugiura, M., Sasamoto, S., Kimura, T., Hosouchi, T., Matsuno, A., Muraki, A., Nakazaki, N., Naruo, K., Okumura, S., Shimpo, S., Takeuchi, C., Wada, T., Watanabe, A., Yamada, M., Yasuda, M., and Tabata, S. (1996) Sequence analysis of the genome of the unicellular cyanobacterium *Synechocystis* sp. strain PCC6803. II. Sequence determination of the entire genome and assignment of potential protein-coding regions. *DNA Res.* **3**, 109–136
14. Muñoz, M.-E., Le Borgne, S., Bolívar, F., and Valle, F. (1997) Molecular cloning of the gene that codes for the pyruvate kinase of *Bacillus subtilis* primary characterization of a strain carrying this gene insertionally inactivated. *Microbiology* **39**, 129–140
15. Muñoz, M.-E. and Ponce, E. (2003) Pyruvate kinase: current status of regulatory and functional properties. *Comp. Biochem. Physiol. Part B* **135**, 197–218
16. Sakai, H. (2004) Possible structure and function of the extra C-terminal sequence of pyruvate kinase from *Bacillus stearothermophilus*. *J. Biochem.* **136**, 471–476
17. Suzuki, K., Ito, S., Shimizu-Ibuka, A., and Sakai, H. (2005) Crystallization and preliminary X-ray analysis of pyruvate kinase from *Bacillus stearothermophilus*. *Acta Crystallogr. Section F* **61**, 759–761
18. Sakai, H. (2005) Mutagenesis of the active site Lysine 221 of the pyruvate kinase from *Bacillus stearothermophilus*. *J. Biochem.* **137**, 141–145
19. Ponce, E., Flores, N., Martinez, A., Valle, F., and Bolivar, F. (1995) Cloning of the two pyruvate kinase isoezyme structural genes from *Escherichia coli*: the relative roles of these enzymes in pyruvate biosynthesis. *J. Bacteriol.* **177**, 5719–5722
20. Otwinowski, Z. and Minor, W. (1996) Processing of X-ray diffraction data collected in oscillation mode. *Methods Enzymol.* **276**, 307–326

21. Matthews, B.W. (1968) Solvent content of protein crystals. *J. Mol. Biol.* **33**, 491–497
22. Collaborative Computational project Number 4. (1994) The CCP4 suite: programs for protein crystallography. *Acta Crystallogr. Section D* **50**, 760–763
23. Brunger, A.T., Adams, P.D., Clore, G.M., DeLano, W.L., Gros, P., Grosse-Kunstleve, R.W., Jiang, J.S., Kuszewski, J., Nilges, M., Pannu, N.S., Read, R.J., Rice, L.M., Simonson, T., and Warren, G.L. (1998) Crystallography & NMR system: a new software suite for macromolecular structure determination. *Acta Crystallogr. Section D* **54**, 905–921
24. Jones, T.A., Zou, J.Y., Cowan, S.W., and Kjeldgaard, M. (1991) Improved methods for building protein models in electron density maps and the location of errors in these models. *Acta Crystallogr. Section A* **47**, 110–119
25. Sarkar, G. and Sommer, S.S. (1990) The 'megaprimer' method of site-directed mutagenesis. *Biotechniques* **8**, 404–407
26. Barik, S. and Galinski, M.S. (1991) 'Megaprimer' method of PCR: increased template concentration improves yield. *Biotechniques* **10**, 489–490
27. Pocalyko, D.J., Carrol, L.J., Martin, B.M., Babbitt, C., and Dunaway-Mariano, D. (1990) Analysis of sequence homologies in plant and bacterial pyruvate phosphate dikinase, enzyme I of the bacterial phosphoenolpyruvate: sugar phosphotransferase system and other PEP-utilizing enzymes. Identification of potential catalytic and regulatory motifs. *Biochemistry* **29**, 10757–10765
28. Nguyen, C.C. and Saier, M.H. Jr. (1995) Phylogenetic analysis of the putative phosphorylation domain in the pyruvate kinase of *B. stearothermophilus*. *Res. Microbiol* **146**, 713–719
29. Murzin, A.G., Brenner, S.E., Hubbard, T., and Chothia, C. (1995) SCOP: a structural classification of proteins database for the investigation of sequences and structures. *J. Mol. Biol.* **247**, 536–540
30. Herzberg, O., Celia, C.H.C., Kapadia, G., McGuire, M., Carroll, L.J., Noh, S.J., and Dunaway-Mariano, D. (1996) Swiveling-domain mechanism for enzymatic phosphotransfer between remote reaction sites. *Proc. Natl Acad. Sci. USA* **93**, 2652–2657
31. Robbins, A.H. and Stout, C.D. (1989) Structure of activated aconitase: formation of the [4Fe-4S] cluster in the crystal. *Proc. Natl Acad. Sci. USA* **86**, 3639–3643
32. DeLano, W.L. (2002) *The PyMOL Molecular Graphics System*, DeLano Scientific, San Carlos, CA, USA.